1   # Cytochrome expression shifts in *Geobacter sulfurreducens* to maximize

2   # energy conservation in response to changes in redox conditions

3   Ethan Howley[a,b], Rosa Krajmalnik-Brown[b,c], César I. Torres[a,d]

4   [a]Biodesign Swette Center for Environmental Biotechnology, Arizona State University – Tempe, AZ

5   [b]School of Sustainable Engineering and the Built Environment, Arizona State University – Tempe, AZ

6   [c]Biodesign Center for Health Through Microbiomes, Arizona State University – Tempe, AZ

7   [d]School for Engineering of Matter, Transport, and Energy, Arizona State University – Tempe, AZ

8

9

10 ## Abstract

11 Previous studies have identified that *Geobacter sulfurreducens* has three different electron

12 transfer pathways for respiration, and it switches between these pathways to adapt to the redox

13 potential of its electron acceptor. However, only a small fraction of the electron carriers from

14 each pathway have been identified. In this study, we combined electrochemical and gene

15 expression data to identify electron carriers associated with each of the three pathways in the

16 inner membrane, periplasm, outer membrane, and exterior of the cell. We demonstrate that it is

17 not just the electron acceptor redox potential that controls pathway expression in *G.*

18 *sulfurreducens*. Our method combining electrochemical modeling and transcriptomics could be

19 adapted to better understand electron transport in other electroactive organisms with complex

20 metabolisms.

1

21 ## Graphical Abstract
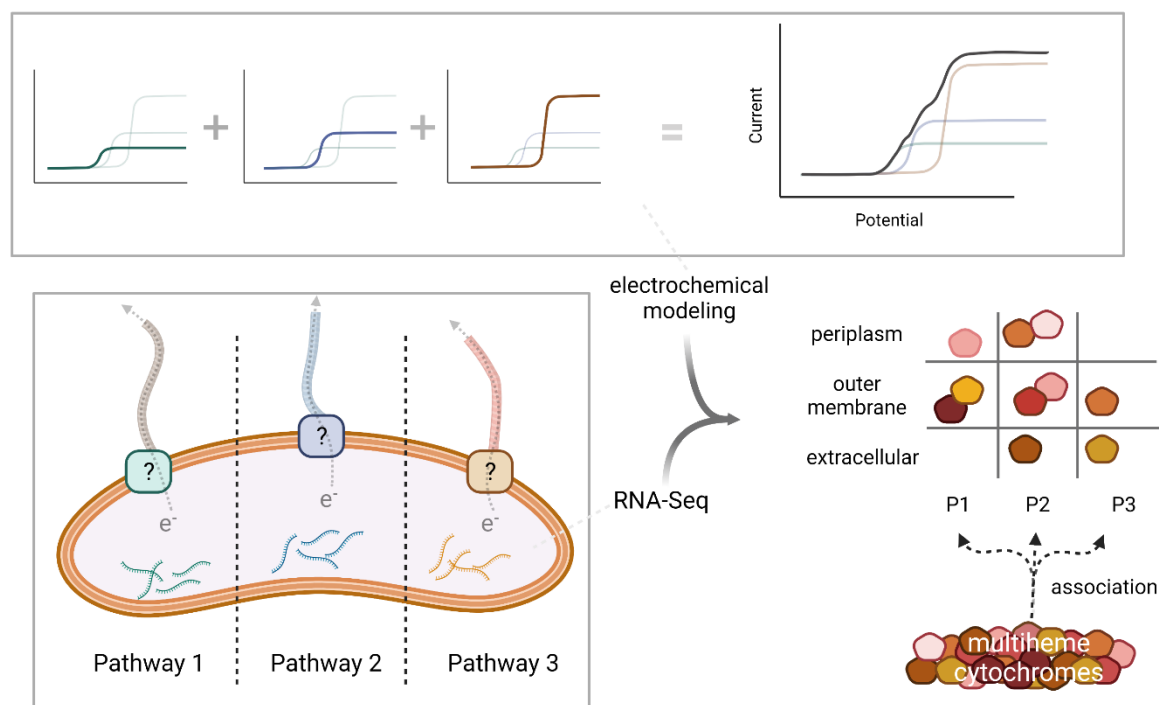
22

23 Graphical abstract was created with Biorender.com

24

25

26 ## Introduction

27 *Geobacter sulfurreducens* is an anaerobic, gram negative, dissimilatory metal reducing

28 bacterium (DMRB) that is important in natural systems as an iron reducer as well as in

29 engineered microbial electrochemical systems as an anode-respiring bacterium (ARB) (Bond and

30 Lovley 2003; Caccavo et al. 1994). It can efficiently reduce various metal oxides with a wide

31 range of redox potentials (Levar et al. 2017; Pat-Espadas et al. 2013; Shelobolina et al. 2007),

32 and this flexibility extends to respiring to an anode where *G. sulfurreducens* is capable of

33 adapting to a range of poised anode potentials (Gao et al. 2018; Yoho, Popat, and Torres 2014).

2

34   The genome of *G. sulfurreducens* contains genes for over 100 putative c-type cytochromes, with

35   more than 70 of those containing multiple heme-binding motifs (Ding et al. 2008). These

36   multiheme cytochromes have been the target of many studies into electron transfer in *G.*

37   *sulfurreducens*, but only a few have been definitively linked to a precisely explained function

38   (Salgueiro et al. 2022). Even well-characterized cytochromes, such as the periplasmic

39   cytochrome PpcA (Pessanha et al. 2006) or the outer membrane complex OmcB (Liu et al.

40   2015), are often known to participate in certain respiratory conditions, but their specific electron

41   donor/acceptor are unknown. As such, the specific electron transport chain pathway for *G.*

42   *sulfurreducens* has been extensively speculated but not well elucidated (Bonanni, Massazza, and

43   Busalmen 2013; Santos et al. 2015).

44   Early transcriptomic and proteomic studies on *G. sulfurreducens* focused on comparing growth

45   with different electron acceptors, particularly between soluble (e.g., fumarate, iron citrate) and

46   solid ones (e.g. anodes, iron oxides). Through these studies, several cytochromes have been

47   confirmed to be important in extracellular respiration. For example, OmcB, OmcS, OmcZ, and

48   other cytochromes were implicated in extracellular electron transfer because their gene

49   transcripts were more abundant in conditions using a solid terminal electron acceptor relative to

50   an insoluble one (Holmes et al. 2006; Nevin et al. 2009). It has been hypothesized that long-

51   range electron transfer in *G. sulfurreducens* was due to some combination of pili and associated

52   cytochromes like OmcZ (Malvankar et al. 2011; Nevin et al. 2009). Recent cryo-electron

53   microscopy studies have shown that the nanowires that *G. sulfurreducens* produce are actually

54   composed of repeating subunits of OmcS or OmcZ, and differences in strain and electron

55   acceptor can alter which protein is dominantly expressed (Wang et al. 2019; Yalcin et al. 2020).

56   More recently, researchers have discovered three elements at the inner membrane that are

57   required for *G. sulfurreducens* to respire at certain potentials, independent of the electron

58   acceptor used. Deleting the inner membrane cytochrome CbcL prevents *G. sulfurreducens* from

59   respiring at electrode potentials below -0.1 V vs. SHE, and deleting the inner membrane

60   cytochrome ImcH prevents *G. sulfurreducens* from respiring at potential above -0.1 V vs. SHE

61   (Levar et al. 2017; Levar, Chan, and Mehta-kolte 2014; Zacharoff, Chan, and Bond 2016).

62   Recently, the protein complex CbcAB has been shown to facilitate respiration at potentials below

63   -0.21 V vs. SHE (Joshi, Chan, and Bond 2021). At the moment, it is unknown how pathway

64   switching occurs, and what other proteins are involved in each pathway. Nonetheless, these

65   studies have shifted the perspective on how pathways are used in *G. sulfurreducens*, where

66   instead of the type of electron acceptor, the potential of such acceptor plays a major role in

67   pathway utilization. By using an anode as the electron acceptor, we can closely control potential

68   and directly measure respiration in real time.

69   Previous work has also investigated how *G. sulfurreducens* adapts to electron acceptors with

70   different potentials through the use of electrochemical signals (Peng and Zhang 2017; Richter et

71   al. 2009; Zhu, Yates, and Logan 2012). Our group used electrochemical techniques to identify

72   and characterize two distinct electrochemical responses dependent on anode potential and

73   hypothesized that *G. sulfurreducens* is using different electron transfer pathways to efficiently

74   adapt to different potentials (Yoho, Popat, and Torres 2014). These distinct signals were later

75   associated to the pathways in which ImcH and CbcL are present (Levar et al. 2014, 2017). The

76   relative magnitude of the signals associated to these pathways would shift within an hour of a

77   potential shift, suggesting a dynamic and complex optimization of respiratory pathways by *G.*

78   *sulfurreducens*. Anode-respiring biofilms of *G. sulfurreducens* exhibit different electrochemical

79   responses during cyclic voltammetry based on the anode potential they have been acclimated to,

80   providing an additional tool to differentiate between biofilms grown at different potentials.

81   In order for *G. sulfurreducens* to efficiently reduce solid electron acceptors at a wide range of

82   redox potentials while conserving energy, it must have a mechanism to change its electron

83   transport chain. Each cytochrome has its own distinct redox potential due to heme orientation

84   and ligands within the overall protein (Pessanha et al. 2006; Pokkuluri et al. 2011), and therefore

85   has an optimal potential (or range of potentials) under which it will accept and donate electrons

86   in a pathway. If the terminal electron acceptor changes potential significantly, the terminal

87   electron transfer protein may no longer be able to donate electrons and a different terminal

88   electron acceptor will be required to continue respiration. Thus, we hypothesized that a shift in

89   the potential of the electron acceptor would not only require shifts in inner-membrane

90   cytochromes, but throughout the whole respiratory pathway. We designed this study to attempt

91   to find periplasmic, outer membrane, and/or extracellular proteins that are associated with *G.*

92   *sulfurreducens* respiration at different redox potentials.

93   We studied wild type *Geobacter sulfurreducens PCA* grown on anodes using electrochemistry

94   and mRNA expression to identify genes that are likely involved in different electron transfer

95   pathways. With cyclic voltammetry (CV) on *G. sulfurreducens* biofilms, we can identify if

96   different pathway signals are present in biofilms grown at different anode potentials, and what

97   typical anode potentials each pathway is associated with. We associated these CV signals with

98   mRNA-Seq transcriptomics to correlate gene expression with the electrochemical data and find

99   genes that may be associated with adaptation to different electron acceptor potentials. Since

100   previous studies have identified the inner membrane elements associated with each pathway, we

101   closely examined the periplasmic, outer membrane, and extracellular electron-transfer proteins

102   that might shift expression as a function of anode potential.

103

Results and Discussion

105   When studying ARB, we can directly measure respiration via chronoamperometry while varying

106   anode potential to create different respiratory conditions. Anode biofilm cyclic voltammograms

107   (CV) on biofilms of *G. sulfurreducens* can be modeled with the Nernst-Monod expression

108   (Torres et al. 2008, 2010) which assumes a single enzymatic step is rate limiting. Additionally,

109   in cases where multiple pathways are being utilized, multiple Nernst-Monod functions have been

110   used (Yoho, Popat, and Torres 2014).

111   Knockout studies have shown that *G. sulfurreducens* has at least three different electron transfer

112   pathways that are each active in only a certain electron acceptor range, and the switch between

113   pathways is likely facilitated by inner membrane cytochromes (Levar et al. 2017). The pathway

114   containing the inner membrane cytochrome ImcH is used at potentials higher than -0.1 V vs.

115   SHE, while the pathway containing the cytochrome CbcL is active at potentials lower than -0.1

116   V vs. SHE (Levar et al. 2014, 2017). Recently, a third pathway was discovered that contains the

117   *bc*-type cytochrome CbcBA which is required for respiration at potentials below -0.21 V vs. SHE

118   (Joshi, Chan, and Bond 2021). We chose the anode potentials in this experiment (-0.17 V, -0.07

119   V, -0.01 V vs. SHE) in an attempt to create conditions that would require different known

120   pathways in *G. sulfurreducens*, and our modeling approach assumes three distinct

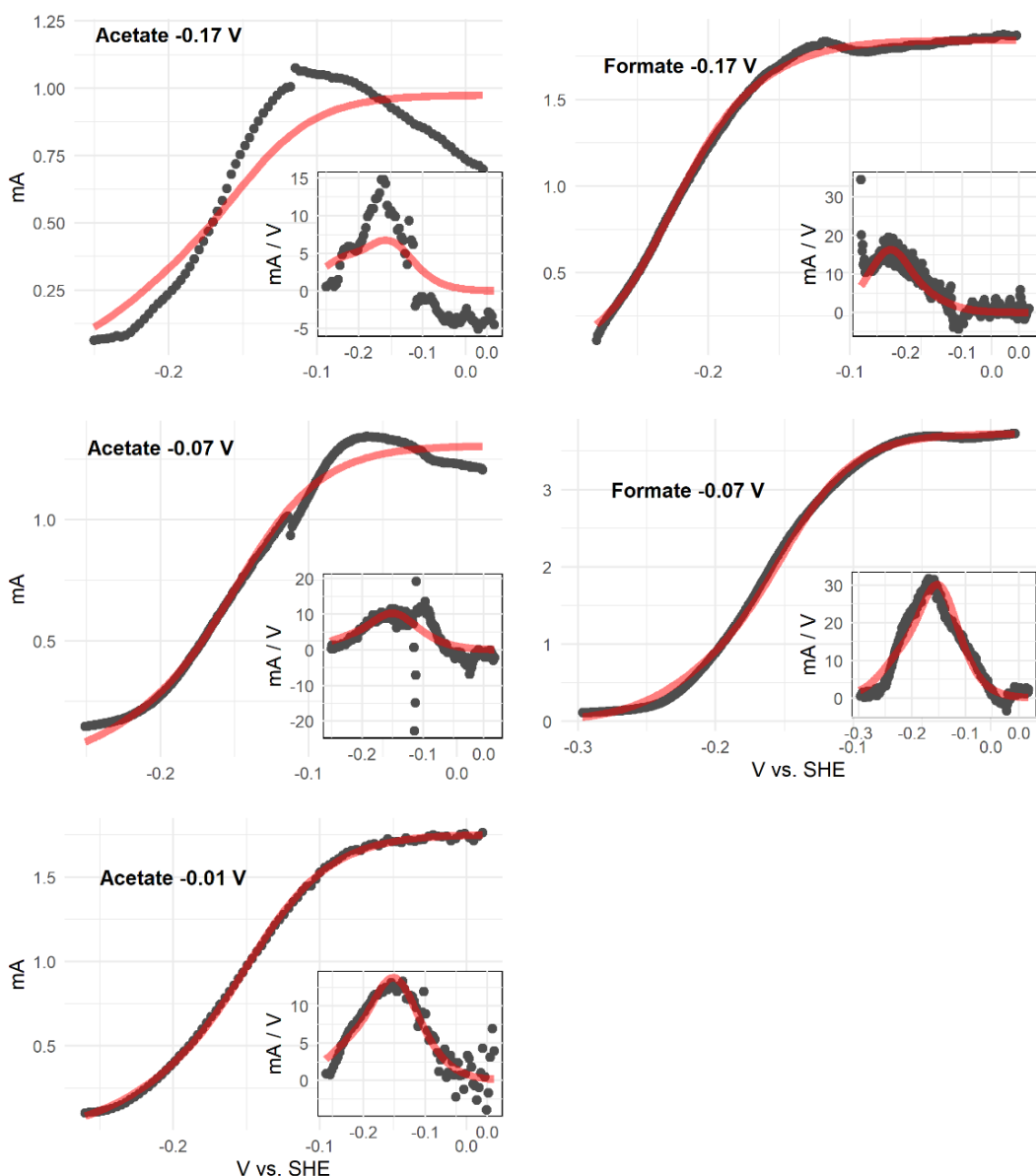121   electrochemical signals in attempt to represent these pathways.

Figure 1: One representative cyclic voltammogram from each condition with its respective

Nernst-Monod model fitting. The experimental data is plotted as gray points, and the model

fitting is the red line. Labels on each plot describe the electron donor used (acetate or formate)

and the fixed anode potential grown at (-0.17 V, -0.07 V, or -0.01 V vs SHE). Inset in each plot

is the differentiation of the CV data (slope) plotted in gray and the derivative of the model fit

function as a red line. Cyclic voltammograms were collected at a scan rate of 5 mV/s at a biofilm

7

129 current density between 1-2 A/m^2 during exponential current increase in order to capture a thin

130 biofilm at a fast enough scan rate to prevent transcriptional adaptation to the shifting potential.

Multiple pathway signals fit to a Nernst-Monod model

132 We were able to approximately fit CVs of the anode biofilm conditions used in this study by

133 adding Nernst-Monod signals with three midpoint potentials: -0.10, -0.15, and -0.227 V vs. SHE;

134 which were selected based on preliminary nonlinear fitting where midpoint was optimized in

135 different conditions (Figure 1). We call these signals High for -0.10 V vs. SHE, Medium for

136 -0.15 V vs. SHE, and Low for -0.227 V vs. SHE. The additive approach to the fitting assumes

137 the signals are utilized simultaneously within the biofilm and cells are not changing expression

138 significantly during the scan. This assumption should be valid with the fast-scan CVs (5 mV/s)

139 we used for fitting, while slower scans are shown to result in pathway shifts within the scan itself

140 (Yoho, Popat, and Torres 2014). With nonlinear fitting, we minimized the error in each fitting by

141 varying the j_{max} coefficient for each E_{KA}. In some cases, such as the Acetate -0.17 V growth

142 condition, fitting had a higher error due to a peak in current density that cannot be estimated by

143 the steady-state assumption of the Nernst-Monod (Torres et al. 2008, 2010). We averaged the

144 fractional contribution of each of the coefficients from biological replicates of the same

145 condition to estimate the contribution of each pathway in that condition (Table 1). Fittings were

146 tested in CVs and the derivative of the CV, having similar outcomes for the fitting.

147 Table 1: Average fractional contribution of each Nernst-Monod function to the overall CV fit in

148 each condition. A larger fraction represents a stronger contribution of a certain pathway to the

149 overall signal, while a fraction close to zero suggests that a certain pathway does not contribute

150 to the overall signal in its respective growth condition. Calculated as $j_{max,i}/\Sigma j_{max,n}$ for each cyclic

151   voltammogram. Numbers in parentheses under each value are the sample standard deviations of

152   each parameter from the number of replicates listed in the 'n' column. The "High", "Medium",

153   and "Low" E_{KA} values represent the midpoint potentials (vs. SHE) of each Nernst-Monod

154   expression that add up to best fit the experimental data.

Electron donor, Anode potential during growth	Fraction of signal from each E_{KA}			n
	Low -0.227 V	*Medium* -0.15 V	*High* -0.10 V	
Acetate, -0.17 V	0.59 (0.28)	0.41 (0.29)	0.00 (0.01)	3
Acetate, -0.07 V	0.29 (0.22)	0.60 (0.21)	0.11 (0.04)	4
Acetate, -0.01 V	0.11 (0.08)	0.75 (0.19)	0.14 (0.15)	3
Formate, -0.17 V	0.85 (0.08)	0.10 (0.01)	0.05 (0.07)	2
Formate, -0.07 V	0.45 (0.27)	0.40 (0.40)	0.14 (0.17)	3

155

156   Our cyclic voltammetry fitting with the Nernst-Monod expression indicates that there is an

157   observable difference in which pathways are contributing most to the overall biofilm CV signal

158   (Table 1). The acetate -0.07 V, acetate -0.17 V, and formate -0.07 V conditions had contributions

159   from the Low and Medium signals with little to no contribution from the High pathway. On the

160   other hand, the CVs from the formate -0.17 V condition were overwhelmingly influenced by the

161   Low signal, and CVs from the acetate -0.01 V condition were mainly fitted with the Medium

162   signal. Even though two of the conditions had an anode potential above -0.1 V, none of the CVs

163   had a major contribution from the High signal (Table 1) although higher growth potentials

164   should have a higher contribution of this pathway. The small contributions of the High signal

165   that we observed may be due to the anode potentials we used being lower than the switch point

166   that would trigger expression of the High pathway. Using the information from this model

167   fitting of our CV data, we can discuss differential expression of electron pathway genes in the

168   context of what pathway they may be more strongly associated with.

169   **Growth conditions affect the overall transcriptome**

170   The main drivers of differential gene expression were the different electron donors and electron

171   acceptors used. The fumarate biofilm and the planktonic fumarate samples are highly

172   differentiated from the anode samples, and among the anode samples there is a clear

173   differentiation between formate and acetate conditions but for acetate there was no clear

174   differentiation based on different anode potentials. All three of the anode biofilms grown on

175   acetate cluster closely together, although there are still some significantly differentially

176   expressed genes. A multi-tab .xlsx file with significantly different genes for all pairwise

177   comparisons is included in the SI. The different anode potentials we used had a small effect on

178   the overall transcriptome of *G. sulfurreducens* grown using acetate, but there is clear separation

179   between the two conditions using formate as the electron donor.
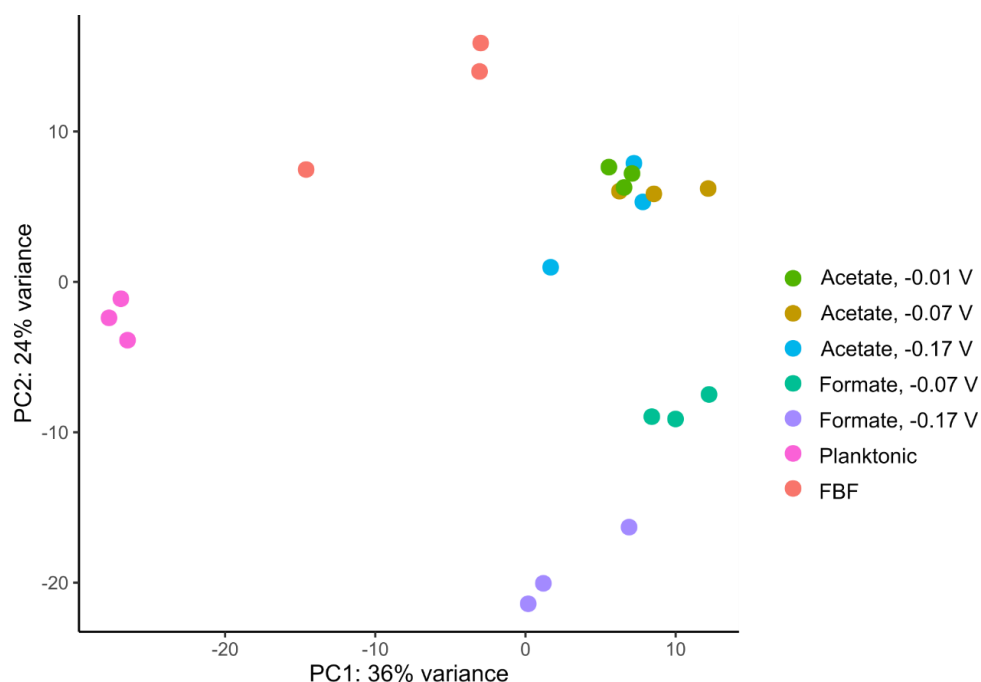
10

Figure 2: PCA plot of variance in expression between triplicate samples grown under seven different electron donor and acceptor conditions. FBF is a fumarate biofilm condition that was grown on an unconnected graphite rod with fumarate as the electron acceptor.
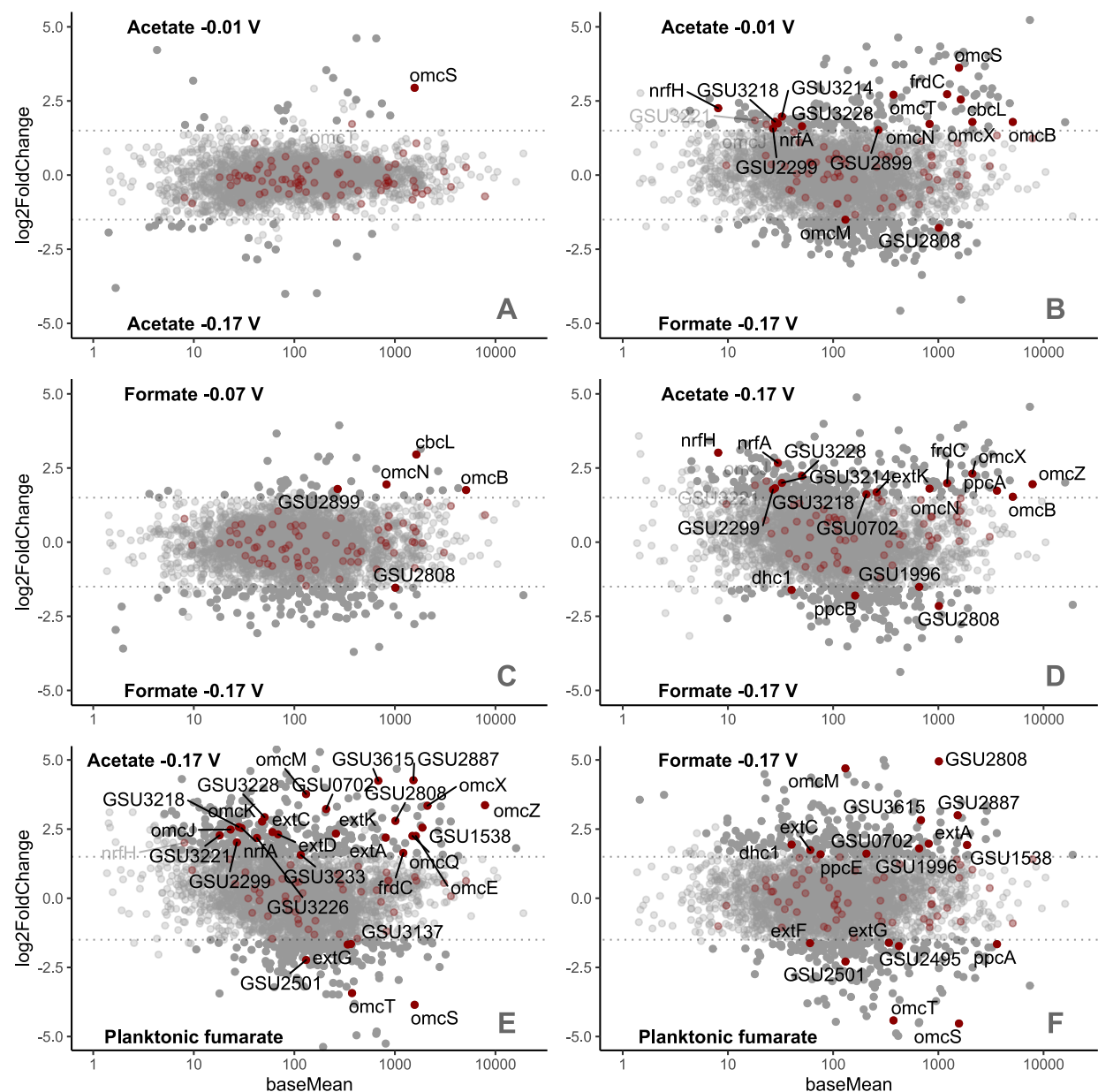
11

Figure 3: MA plots highlighting interesting pairwise comparisons of differential gene expression with multiheme cytochromes highlighted in red. Labels at top and bottom indicate conditions plotted for comparison. Dotted lines are at ±1.5 $\log_2$ fold change, and all clearly labeled genes meet an adjusted p-value <0.05. Base mean is calculated using Deseq2's method for normalizing counts across samples and p values were corrected by the Benjamini Hochberg method. Table 2 lists all the highlighted genes and the associated pathways and cellular locations.

192 Table 2: Multiheme cytochromes with significant differential expression and electrochemical

193 data suggesting an association to one of the three EET pathways. These associations were

194 inferred from the differential expression comparisons in Figure 3, and the electrochemical

195 modeling in Table 1. We assume the fumarate samples exhibit primarily the High pathway due to

196 the relatively high redox potential of the fumarate/succinate couple. *extJ* is not a multiheme c-

197 type cytochrome, but we include it here due to its presence in the ExtHIJK cluster.

Gene		Pathway	Location	Comparisons
ppcB	GSU0364	Low	Periplasmic[c]	Fig. 3D
GSU1538	GSU1538	Low	Periplasmic[a]	Fig. 3E, Fig. 3F
ppcE	GSU1760	Low	Periplasmic[c]	Fig. 3F
GSU1996	GSU1996	Low	Periplasmic[b]	Fig. 3D, Fig. 3F
OmcM	GSU2294	Low	unknown	Fig. 3B, Fig. 3F
extC	GSU2643	Low	Outer Membrane[e]	Fig. 3E, Fig. 3F
extA	GSU2645	Low	Periplasmic[a]/ OM[e]	Fig. 3E, Fig. 3F
dhc1	GSU2767	Low	Inner membrane[a]	Fig. 3D, Fig. 3F
GSU2808	GSU2808	Low	unknown	Fig. 3B, Fig. 3D, Fig. 3E, Fig. 3F
GSU2887	GSU2887	Low	Extracellular[a]	Fig. 3E, Fig. 3F
GSU3615	GSU3615	Low	Extracellular[a]	Fig. 3E, Fig. 3F
cbcL	GSU0274	Medium	inner membrane[f]	Fig. 3B, Fig. 3C
omcQ	GSU0592	Medium	Cytoplasmic[a]	Fig. 3E
ppcA	GSU0612	Medium	Periplasmic[a]	Fig. 3D
omcX	GSU0670	Medium	Periplasmic[a]	Fig. 3B, Fig. 3D, Fig. 3E
omcJ	GSU0701	Medium	unknown	Fig. 3E
GSU0702	GSU0702	Medium	Extracellular[a]	Fig. 3E, Fig. 3F
frdC	GSU1176	Medium	inner membrane[a]	Fig. 3B, Fig. 3D, Fig. 3E
omcZ	GSU2076	Medium	Extracellular[d]	Fig. 3D, Fig. 3E
omcK	GSU2203	Medium	Periplasmic[a]	Fig. 3E
GSU2299	GSU2299	Medium	Periplasmic[a]	Fig. 3B, Fig. 3E

13

omcB	GSU2737	Medium	unknown	Fig. 3B, Fig. 3C, Fig. 3D
omcN	GSU2898	Medium	Periplasmic[a]	Fig. 3B, Fig. 3C, Fig. 3D
GSU2899	GSU2899	Medium	Extracellular[a]	Fig. 3B, Fig. 3C
extK	GSU2937	Medium	Outer Membrane[e]	Fig. 3D, Fig. 3E
extJ	GSU2938	Medium	Outer Membrane[e]	Fig. 3D, Fig. 3E (not labeled)
nrfA	GSU3154	Medium	Periplasmic[a]	Fig. 3B, Fig. 3D, Fig. 3E
nrfH	GSU3155	Medium	Periplasmic[a]	Fig. 3B, Fig. 3D
GSU3214	GSU3214	Medium	unknown	Fig. 3D
GSU3218	GSU3218	Medium	Periplasmic[a]	Fig. 3A, Fig. 3D, Fig. 3E
GSU3221	GSU3221	Medium	unknown	Fig. 3E
GSU3226	GSU3226	Medium	unknown	Fig. 3E
GSU3228	GSU3228	Medium	unknown	Fig. 3B, Fig. 3D, Fig. 3E
GSU3233	GSU3233	Medium	Periplasmic[a]	Fig. 3E
GSU702	GSU702	Medium	Extracellular[a]	Fig. 3D, Fig. 3E Fig. 3F
omcS	GSU2504	High, Fumarate	Extracellular[g]	Fig. 3A, Fig. 3B, Fig. 3E, Fig. 3F
omcT	GSU2503	High, Fumarate	Periplasmic[a]	Fig. 3B, Fig. 3E, Fig. 3F
GSU2501	GSU2501	Fumarate	Periplasmic[a]	Fig. 3E, Fig. 3F
extG	GSU2724	Fumarate	Periplasmic[e]	Fig. 3E, Fig. 3F
extF	GSU2725	Fumarate	Outer Membrane[e]	Fig. 3F

198   a: PSORTb v3.0, b: (Pokkuluri et al. 2011), c: (Morgado et al. 2010), d: (Inoue et al. 2010), e: (Jiménez Otero et al.

199   2021), f: (Zacharoff, Chan, and Bond 2016), g: (Wang et al. 2019)

200

201   EET pathways in *G. sulfurreducens* are populated with multiheme cytochromes – some known

202   and some unknown. By synthesizing the modeling outputs from our CV data (Table 1) and the

203   differential gene expression of multiheme cytochromes in important pairwise comparisons

14

204   (Figure 3), we can create associations between cytochromes and electrochemical pathways

205   (Table 2).

Membrane cytochromes can be associated to a specific pathway

207   Four clusters of outer membrane genes have been shown to be required for EET in *G.*

208   *sulfurreducens* under certain conditions: ExtABCD, ExtEFG, ExtHIJK, and OmcBC; deleting all

209   four clusters prevents EET respiration (Otero and Chi Ho Chan 2018). Our differential

210   expression data suggests that these clusters may be associated with different electron acceptor

211   potentials. In our data, *extJ* and *extK* were downregulated in the formate -0.17 V biofilm versus

212   the acetate -0.17 V biofilm ($\log_2$FC=2.6, p_{adj}=0.016, $\log_2$FC=1.7, p_{adj}=0.016). The formate -0.17

213   V biofilm was predominantly represented by the Low pathway in our electrochemical data

214   whereas the acetate -0.17 V biofilm had a strong signal from the Medium pathway. From this, we

215   can infer that the ExtHIJK proteins may contribute to the Medium pathway signal. SHE.

216   Likewise, we infer that ExtEFG may be associated with respiration at the highest potentials due

217   to the downregulation of *extF* and *ExtG* in the formate condition grown at an electrode potential

218   of -0.17 V when compared to the expression in planktonic fumarate sample which we assume

219   represents expression of the pathway associated with the highest potential. The

220   fumarate/succinate redox couple has a standard potential of 0.03 V at pH 7, making it more

221   positive than any other acceptor used in this study.

222   The expression of the gene *omcB* is downregulated in the formate -0.17 V biofilm relative to the

223   acetate anode biofilms at all three potentials and the formate -0.07 V biofilm, indicating that it

224   may be associated with the Medium pathway. OmcB forms part of a conduit that transfers

225   electrons through the outer membrane and is involved in reduction of Fe(III) citrate and

15

226   ferrihydrite (Liu et al. 2015). We observed differential expression of OmcB but not OmcC – two

227   paralogs with 65% amino acid similarity. *GSU2808* is another outer membrane cytochrome with

228   the opposite expression pattern to *omcB*. *GSU2808* was significantly upregulated in the formate

229   –0.17 V biofilm relative to all other anode biofilm conditions indicating an association with the

230   Low pathway. *GSU2808* is a 5 heme cytochrome that has been linked to palladium reduction

231   with acetate as the electron donor (Hernández-Eligio et al. 2020).

232   We expected to see upregulation of *imcH*. ImcH is the inner membrane cytochrome required for

233   EET at anode potentials above –0.1 V vs. SHE, but there was no significant change among any

234   anode potentials. Yet, *imcH* was a highly expressed cytochrome gene in all conditions, with a

235   base mean of 869 which is in the 94th percentile among all genes. Given the anode potentials we

236   chose, it is possible that our experimental design did not capture the differential expression of

237   *ImcH*. Based on our electrochemical modeling and the differential expression data, none of the

238   conditions we studied were primarily using the High pathway associated to *ImcH* (Table 1,).

239   CbcL, the inner membrane cytochrome required for potentials below –0.1 V vs. SHE, was

240   significantly downregulated in the formate –0.17 vs. SHE samples compared to the formate –0.07

241   V samples (log2FC = 3.0, adjusted p = 1.8E-5) but not significantly different between any of the

242   acetate anode biofilm potentials. This observation fits well with the CV data where all conditions

243   except for the –0.17 V formate biofilm had a signal from the Medium pathway. Recent work has

244   identified CbcAB as a crucial protein complex for *G. sulfurreducens* to respire at potentials

245   below –0.2 V vs. SHE (Joshi et al preprint 2021), but we did not detect any differential

246   expression in *cbcA* or *cbcB*, although each gene had a base mean of counts in the 97th and 95th

247   percentile, respectively. Apart from these known inter membrane proteins, *dhc1* was

248   differentially expressed with an association to the Low potential condition (Table 2). This gene

16

249 encodes for a unique diheme cytochrome of unknown function with a predicted inner membrane

250 localization.

Extracellular cytochromes network adapts to redox conditions

252 Filaments made of OmcS or OmcZ units have been implicated as a critical component of long

253 distance EET (Wang et al. 2019; Yalcin et al. 2020). We observed that *omcS* was significantly

254 upregulated in the fumarate conditions relative to all anode biofilms except for the acetate -0.07

255 V vs. SHE condition. *G. sulfurreducens* may use OmcS for EET only at higher anode potentials,

256 above ~ (−0.1) V vs. SHE. Fumarate, with a standard reduction potential of 0.03 V vs. SHE,

257 appears to be stimulating the expression of the High pathway. To our knowledge, previous

258 studies on OmcS filaments have all used either fumarate or an electrode poised above 0 V vs.

259 SHE as the electron acceptor. Of the "*omc*" genes, the most likely candidate for replacing the

260 function of OmcS at lower potentials based on our data is *omcZ*. The OmcZ protein was recently

261 shown to form nanowires with a high conductivity in *G. sulfurreducens* (Yalcin et al. 2020) and

262 has been shown to be preferentially expressed at low potentials (Peng and Zhang 2017). Our data

263 supports that the differential expression of *omcS* vs. *omcZ* appears to be at least partially

264 controlled by electron acceptor potential with *omcZ* being important when the Medium pathway

265 is detected. Interestingly, we did not observe an upregulation of *omcZ* in the Formate -0.17 V

266 condition relative to planktonic fumarate despite the down regulation of *omcS* (Figure 3B and

267 3F), suggesting that there may be more than just *omcS* and *omcZ* responsible for the pathway-

268 dependent switch in the extracellular part of the pathway. Other cytochromes with predicted

269 extracellular localization (GSU2887, GSU3615) were more abundantly expressed under the Low

270 Pathway conditions, but the function of these cytochromes is yet to be elucidated (Kim et al.

271 2005; Leang et al. 2005; Peng et al. 2016)

17

272 **Differential expression of Ppc proteins may maximize respiratory efficiency**

273 Five periplasmic triheme cytochromes (PpcA-E) have been identified and characterized in *G.*

274 *sulfurreducens* (Lloyd et al. 2003). PpcA was first characterized and shown that its deletion

275 affects Fe(III) and U(VI) reduction, but not fumarate reduction. PpcB-D were initially identified

276 due to their high similarity to PpcA (75-100%), while predictions confirmed their periplasmic

277 location (Shelobolina et al. 2007). Most studies have suggested the role of these cytochromes is

278 to transfer electrons collected at the inner membrane to outer-membrane cytochromes (Lloyd et

279 al. 2003; Morgado et al. 2010; Shelobolina et al. 2007). Interestingly, further studies have

280 confirmed that PpcA and PpcD perform a proton-coupled electron transfer; which leads to the

281 possibility that these periplasmic cytochromes are associated to ATP production (Morgado et al.

282 2010). It has also been confirmed that electron transfer by PpcB and PpcE are not proton

283 coupled, suggesting a different cellular function compared to PpcA/PpcD (Silva, Portela, and

284 Salgueiro 2021).

285 Our observed gene expression for Formate at -0.17 V vs SHE, which has primarily the Low

286 pathway evident, shows an increased expression of PpcB (Fig. 3D) and PpcE (Fig. 3F) over

287 PpcA compared to conditions where the Medium pathway is active. Our study associates the use

288 of PpcB and PpcE to the Low pathway. On the other hand, *ppcA* seems to be highly expressed in

289 all other samples, this suggests its utilization for the Medium and/or High pathways. Given that

290 the lower potential pathway is associated with lower electron-transfer energy available in *G.*

291 *sulfurreducens* metabolism, there is limited energy for proton pumping and ATP production.

292 The use of PpcB/PpcE could be an approach to decrease ATP production when the energy

293 gradient is limiting, while PpcA is used when more energy is available. Thus, our results are

294 consistent with the hypotheses that PpcA/PpcD are associated with ATP production (Morgado et

18

295   al. 2010; Silva, Portela, and Salgueiro 2021). Analyses of these periplasmic cytochromes have

296   also discussed differences in working potentials, which could indicate different electron

297   acceptors (Morgado et al. 2010). The PpcA-E proteins function as periplasmic electron carriers

298   in *G. sulfurreducens'* EET, so a change in the distribution of the different Ppc proteins could

299   allow *G. sulfurreducens* to maintain efficiency as external redox conditions change.

300   We also observed differential expression of several large cytochromes, each with at least a dozen

301   hemes. *GSU3218* (15 hemes), *GSU0702* (35 hemes), and *omcN* (34 hemes) are upregulated in

302   the acetate -0.17 V condition relative to the formate -0.17 V condition, and therefore we

303   associate them with the Medium pathway (Table 2). *GSU0702* has been previously associated

304   with respiration of electrodes at lower potentials as it was upregulated in *G. sulfurreducens*

305   grown at -0.25 V vs. SHE compared to +0.2 V (Peng et al. 2016). Deleting *omcN* does not

306   impact the reduction of soluble or insoluble electron acceptors in one study (Aklujkar et al.

307   2013). The 27-heme cytochrome gene *GSU2887* is associated with the Low pathway. The

308   proteins encoded by *GSU2887* and *GSU0702* are both predicted to be extracellular by PSORTb

309   3.0, but it is not clear what the function of such large cytochromes would be outside the cell.

310   **Formate metabolism suppresses the TCA cycle**

311   When acetate is available, *Geobacter* uses NADH generated from the TCA cycle to pump

312   protons across the membrane using NADH dehydrogenase for energy conservation. When

313   formate is the only electron donor available, *Geobacter* suppresses the TCA cycle and shifts to

314   an alternate metabolism. There were 80 genes differentially expressed between *G.*

315   *sulfurreducens* anode biofilms grown with the same -0.07 V vs. SHE potential with either acetate

316   or formate as the electron acceptor. Ten genes encoding for subunits of the NADH

19

317   dehydrogenase complex were significantly downregulated in the formate condition. Every gene

318   encoding for an enzyme in the TCA cycle except for *sucA*, 2-oxoglutarate dehydrogenase, was

319   downregulated in the formate samples. In the formate condition, we observed the upregulation of

320   15 genes including *fdhD* (formate dehydrogenase) (Supplemental spreadsheet). The

321   downregulation of NADH dehydrogenase (*nuo* genes) and the upregulation of formate

322   dehydrogenase that we observe in formate biofilms indicate that formate dehydrogenase is

323   replacing NADH dehydrogenase as the primary electron carrier in the membrane electron

324   transfer chain. There is no evidence that *Geobacter*'s formate dehydrogenase can pump protons

325   in the same way as NADH dehydrogenase.

326   Formate may stimulate a similar response as hydrogen in *Geobacter*. *hgtR*, the hydrogen-

327   dependent growth transcriptional regulator, is a critical protein for shifting metabolism to use

328   hydrogen as the electron donor (Ueki and Lovley 2009). Joshi, Chan, and Bond 2021 also found

329   that *hgtR* is upregulated in a mutant *G. sulfurreducens* where an upstream regulator of CbcAB is

330   deleted (Δ*bccR*), potentially because of thermodynamic limitations on respiration. We observed

331   upregulation of *hgtR* in both formate biofilms relative to all acetate conditions except for the

332   acetate -0.01 V biofilm. Although we did observe downregulation of the TCA cycle in formate

333   conditions, the fact that *hgtR* was also relatively highly expressed in the -0.01 V acetate biofilm

334   suggests that it is not solely related to hydrogen/formate metabolism, but instead a

335   thermodynamic response in *G. sulfurreducens*. It is also possible that small amounts of hydrogen

336   were produced in our single-chamber reactors, and this activated *hgtR*, but in that case we would

337   not expect to see differential expression as a function of potential or electron donor.

338

339   We initially chose to study conditions where fumarate was the electron acceptor to capture the

340   transcriptome of cells that did not need to use EET. Instead, we observed the expression of many

341   of the EET-associated proteins in the fumarate conditions. Our data support other work that has

342   shown that *G. sulfurreducens* is not optimized to grow with fumarate. OmcS nanowires have

343   been isolated from fumarate cultures of *G. sulfurreducens* (Wang et al. 2019), indicating that

344   fumarate cultures produce the machinery of the High potential EET pathway. *G. sulfurreducens*

345   also prefers Fe(III) as an electron acceptor when both Fe(III) and fumarate are available despite

346   fumarate providing more energy (Esteve-Núñez, Núñez, and Lovley 2004). *G. sulfurreducens*

347   uses a reversible enzyme complex, FrdCAB for both fumarate reduction during fumarate

348   respiration and succinate dehydrogenation as part of the TCA cycle (Butler et al. 2006). In our

349   data *frdC* was differentially expressed, although it was not correlated with fumarate utilization.

350   Rather, fumarate reductase was regulated along with the other elements of the TCA cycle. *frdC*

351   was downregulated in the formate conditions relative to the acetate biofilms which is consistent

352   with the downregulation of the other TCA cycle enzymes. We did, however, observe an

353   increased expression of *dcuB* in fumarate conditions. DcuB is the fumarate transporter in *G.*

354   *sulfurreducens* (Butler et al. 2006).

355

356   Conclusion

357   Due to its complicated electron pathways, fully understanding EET in *G. sulfurreducens* will

358   require synthesizing data from many techniques, and a large body of literature. In this study, we

359   combined electrochemical CV fittings using Nernst-Monod modeling and RNASeq to identify

360   electrochemical conditions that change the expression of genes associated with different

361   pathways. We have identified a number of genes that show an association to different respiratory

362   pathways in *G. sulfurreducens*, and this technique could be expanded in further studies to answer

363   more unresolved questions about the metabolism of *G. sulfurreducens* and other electroactive

364   organisms.

365   Over decades of research in *G. sulfurreducens*, expression studies have often assumed an anode,

366   often poised at high potentials, as a fixed condition for growth; only recently have studies started

367   to recognize the importance of shifting anode potentials in its expression and electrochemical

368   behavior (Levar et al. 2017; Peng et al. 2016). Our results suggest that a small shift in the anode

369   potential (100-160 mV in our study) cause significant changes in the respiratory pathway of *G.*

370   *sulfurreducens*. While this is a small potential change, it constitutes a significant increase (87-

371   139%) in available energy for growth using acetate as electron donor ($E^{0'} = -285$ mV vs SHE). It

372   seems that changes along the full electron path, from the inner membrane to the extracellular

373   matrix, occur because of a change in potential. In Figure 4, we hypothesize an updated model of

374   EET in *G. sulfurreducens*. Trifurcation of electrons occurs at the inner membrane as previously

375   reported (Joshi, Chan, and Bond 2021; Levar et al. 2017). In order to maintain efficient energy

376   conservation, many redox proteins along the EET pathway should change to create a cascading

377   potential gradient from the inner membrane to the anode. Based on our data, we propose in

378   Figure 4 some of the electron carriers in each of the three pathways, with changes at the

379   periplasmic, outer membrane, and extracellular portions of the electron transfer chain. We

380   anticipate that future studies will associate more electron carriers with each pathway and

381   complete the model.

382   Since the respiratory pathways in *G. sulfurreducens* involve a complex network of cytochromes

383   extending to the extracellular space, changing this pathway due to a shift in electron acceptor

384   conditions (e.g., change in anode or metal oxide potential) would require a significant energy

385   investment. Thus, our results imply some limitations in respiratory efficiencies as redox

386   conditions change and add more context to the complicated story of *G. sulfurreducens*.
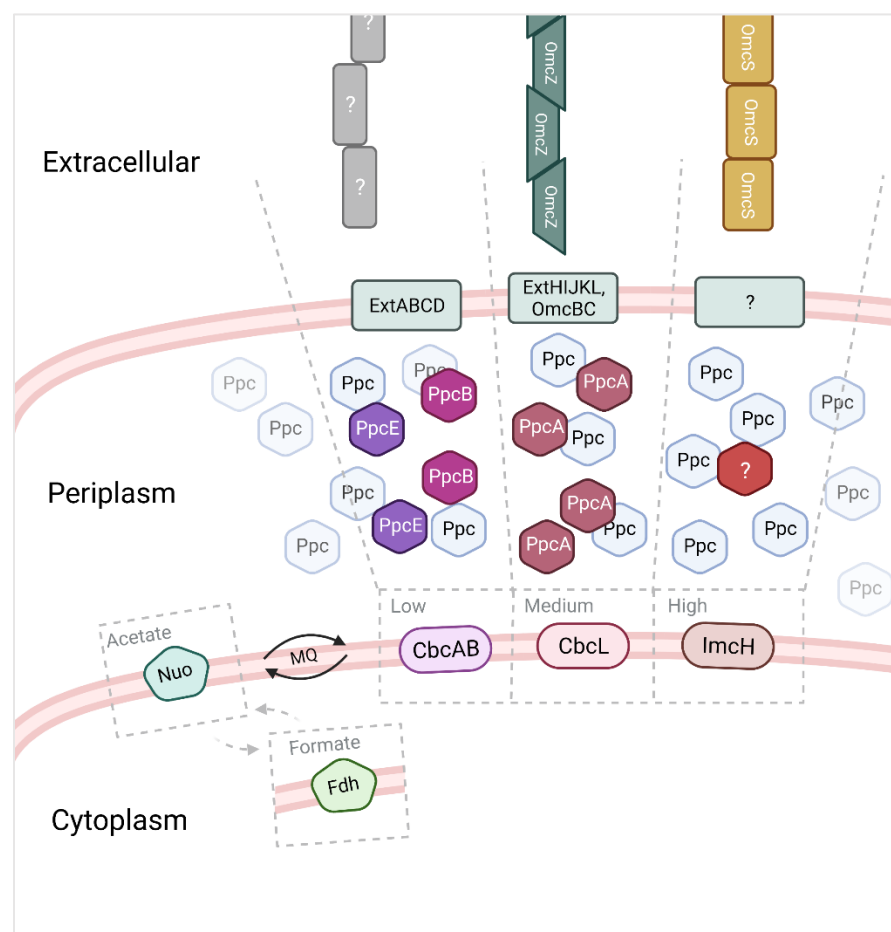
387

388   Figure 4: Our hypothesized schematic of the EET process in *G. sulfurreducens* and how it is

389   differentiated based on electron acceptor potential. At the inner membrane NADH

390   dehydrogenase (Nuo) reduces menaquinone (MQ), or in the case of formate metabolism Nuo is

391   downregulated and formate dehydrogenase (Fdh) initializes the inner membrane electron transfer

392   chain. At the inner membrane, electrons enter one of three EET pathways. In the Low pathway,

393   CbcAB (Joshi, Chan, and Bond 2021) oxidizes menaquinol, the periplasmic electron transfer

394   favors PpcB and PpcE, and the ExtABCD complex is involved at the outer membrane. In the

23

395   Medium pathway, CbcL transfers electrons to PpcA in the periplasm and then to ExtHIJKL and

396   OmcBC and OmcZ at the outer membrane. Our study did not capture the High pathway well, but

397   we do know it uses ImcH (Levar et al. 2017) at the inner membrane and OmcS as an

398   extracellular electron carrier. This diagram is not a complete explanation of all the EET

399   pathways in *G. sulfurreducens* but rather a way to highlight some of the associations we have

400   discovered. Created with BioRender.com.
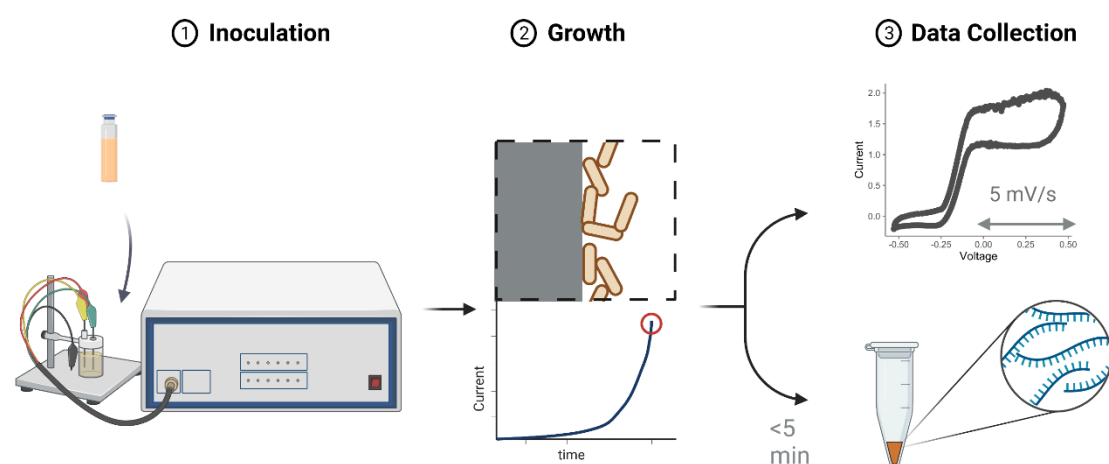
401

402   Methods

403

404

405   <u>Figure 5:</u> 1) *G. sulfurreducens* is inoculated into a microbial electrochemical cell with a graphite

406   electrode acting as the electron acceptor for growth using a potentiostat to apply a potential. 2)

407   Growth is monitored via chronoamperrometry until the bacteria produce 1-2 A/m^2 during

24

408   exponential growth, indicating a thin and active biofilm. 3) At this stage, we perform cyclic

409   voltammetry on the biofilm, or the biofilm is collected, and RNA is extracted for

410   transcriptomics. Created with BioRender.com.

411   **Growth**

412   *Geobacter sulfurreducens* PCA was grown under 7 different conditions. "Planktonic" samples

413   used ATCC 1957 medium in sealed anaerobic test tubes and extracted 48 hours after inoculation.

414   Anode biofilm samples used a modified ATCC 1957 medium without sodium fumarate in a

415   single chamber microbial electrochemical cell with a graphite rod electrode ($600\text{-}800\text{mm}^2$)

416   serving as an anode. The reactor volume was 100mL with an Ag/AgCl reference electrode

417   (BASi, Indiana USA) and a stainless-steel wire as cathode. Acetate anode biofilms were poised

418   at three different potentials, -0.07 V vs. SHE, -0.17 V vs. SHE, and -0.01 V vs. SHE. Formate

419   anode biofilms were poised at two potentials – -0.07 V vs. SHE, and -0.17 V vs. SHE. We used a

420   conversion of -0.27 V vs. Ag/AgCl is 0 V vs. SHE. Anode biofilm growth was monitored with a

421   BioLogic VMP3 potentiostat (Tennessee, USA) and samples were collected during exponential

422   current growth phase in the range of 1-3 A/m^2 to capture a thin biofilm. Fumarate biofilm

423   samples used ATCC 1957 medium in a continuously mixed flow-through reactor identical to the

424   anode biofilm reactor with a hydraulic retention time less than the reported doubling time for *G.*

425   *sulfurreducens* and with the cell in open circuit. Planktonic samples were collected by

426   centrifugation, and biofilms were collected by scraping. Seven conditions were sampled in

427   biological triplicate for a total of twenty-one samples.

428   **RNA processing**

25

429   RNA was extracted from all samples with a QIAGEN PowerMicrobiome RNA extraction kit

430   (Germany). The extraction process began within 5 minutes of disturbing each culture. RNA

431   quality and quantity were assessed with a Nanodrop spectrophotometer and an Agilent

432   Bioanalyzer 2100. Ribosomal RNA contamination was reduced with the MICROBExpress

433   Bacterial mRNA enrichment kit (ThermoFisher, Massachusetts USA). Illumina (California

434   USA) sequencing libraries were prepared with KAPA Biosystems Hyperprep RNA

435   (Massachusetts USA) before pooling and sequencing on an Illumina Nextseq 500 2x150 module.

436   Sequencing was performed at the OKED Genomics Core at Arizona State University.

437   **Differential Expression**

438   Sequence quality was assessed with FastQC (Andrews 2010). After demultiplexing, reads were

439   trimmed with trimmomatic (Bolger, Lohse, and Usadel 2014) to remove low quality read

440   segments. The majority of ribosomal reads were removed by alignment to reference sequences in

441   Bowtie2 Filtered reads were aligned to the *G. sulfurreducens* PCA RefSeq genome using

442   Bowtie2 (Langmead and Salzberg 2012), and only paired alignments were kept. Alignment files

443   were transformed for analysis in R with samtools (Li et al. 2009). In R, aligned reads were

444   mapped to the NCBI RefSeq assembly for *G. sulfurreducens*. Ribosomal RNA-mapped reads

445   were removed before differential expression analysis. Differential gene expression was analyzed

446   with the R package DESeq2 (Love, Huber, and Anders 2014). Ribosomal protein genes are

447   removed from data presented here. Transcriptomic data and metadata are hosted in the NCBI

448   Gene Expression Omnibus database under accession number GSE200066.

449   **Electrochemistry**

450   Anode biofilms used for cyclic voltammetry were grown under similar conditions to the samples

451   used for RNA extraction. We used a Bio-Logic VMP3 potentiostat for all chronoamperometry

452   and cyclic voltammetry. Cyclic voltammograms were recorded with a scan rate of 5 mV/s from

453   −0.5 V vs. SHE to +0.5 V vs SHE. A total of 3 consecutive scans were performed for each

454   biofilm and the second scan was used for fittings. Fitting to Nernst-Monod curves to the data by

455   optimizing each j_{max} was performed in using the nl2sol non-linear least squares regression from

456   the R package stats (R 3.6.3, 2021).

457   $$j = j_{1_{max}} \left(\frac{1}{1 + \exp\left(-\frac{F}{RT}(E - E_{KA_1})\right)} \right) + j_{2_{max}} \left(\frac{1}{1 + \exp\left(-\frac{F}{RT}(E - E_{KA_2})\right)} \right) + j_{3_{max}} \left(\frac{1}{1 + \exp\left(-\frac{F}{RT}(E - E_{KA_3})\right)} \right)$$

458   Equation 1: Three-part Nernst-Monod expression to model the *G. sulfurreducens* biofilm cyclic

459   voltammograms. F is Faraday's constant (96,485 C/mol), R is ideal gas law constant (−8.314

460   J/mol K, T is temperature (K), and E is the anode potential (V) as measured by the potentiostat. j

461   is current density (A/m^2). In the model, each $j_{i,max}$ was a fitting parameter.

462

463   **Acknowledgements**

466

467

468

469

27

470 **References**

471 Aklujkar, M. et al. 2013. "Proteins Involved in Electron Transfer to Fe(III) and Mn(IV) Oxides

472   by Geobacter Sulfurreducens and Geobacter Uraniireducens." *Microbiology (United*

473   *Kingdom)* 159(PART3): 515–35.

474 Andrews, S. 2010. "FastQC: A Quality Control Tool for High Throughput Sequence Data

475   [Online]." http://www.bioinformatics.babraham.ac.uk/projects/fastqc/.

476 Bolger, Anthony M., Marc Lohse, and Bjoern Usadel. 2014. "Trimmomatic: A Flexible Trimmer

477   for Illumina Sequence Data." *Bioinformatics* 30(15): 2114–20.

478 Bonanni, Pablo Sebastián, Diego Massazza, and Juan Pablo Busalmen. 2013. "Stepping Stones

479   in the Electron Transport from Cells to Electrodes in Geobacter Sulfurreducens Biofilms."

480   *Physical Chemistry Chemical Physics* 15(25): 10300–306.

481 Bond, Daniel R., and Derek R. Lovley. 2003. "Electricity Production by Geobacter

482   Sulfurreducens Attached to Electrodes." *AEM* 69(3): 1548–55.

483 Butler, Jessica E et al. 2006. "Genetic Characterization of a Single Bifunctional Enzyme for

484   Fumarate Reduction and Succinate Oxidation in Geobacter Sulfurreducens and Engineering

485   of Fumarate Reduction in Geobacter Metallireducens." 188(2): 450–55.

486 Caccavo, Frank et al. 1994. "Geobacter Sulfurreducens Sp. Nov., a Hydrogen- and Acetate-

487   Oxidizing Dissimilatory Metal-Reducing Microorganism." *Applied and environmental*

488   *microbiology* 60(10): 3752–59.

489 Clarke, T. A. et al. 2011. "Structure of a Bacterial Cell Surface Decaheme Electron Conduit."

490   *Proceedings of the National Academy of Sciences* 108(23): 9384–89.

491   http://www.pnas.org/cgi/doi/10.1073/pnas.1017200108.

492   Ding, Yan Huai R et al. 2008. "Proteome of Geobacter Sulfurreducens Grown with Fe(III) Oxide

493   or Fe(III) Citrate as the Electron Acceptor." *Biochimica et Biophysica Acta - Proteins and*

494   *Proteomics* 1784(12): 1935–41. http://dx.doi.org/10.1016/j.bbapap.2008.06.011.

495   Esteve-Núñez, Abraham, Cinthia Núñez, and Derek R. Lovley. 2004. "Preferential Reduction of

496   Fe(III) over Fumarate by Geobacter Sulfurreducens." *Journal of Bacteriology* 186(9):

497   2897–99.

498   Gao, Yifan et al. 2018. "Urine-Powered Synergy of Nutrient Recovery and Urine Purification in

499   a Microbial Electrochemical System." *Environmental Science: Water Research and*

500   *Technology* 4(10): 1427–38.

501   Hernández-Eligio, Alberto et al. 2020. "Global Transcriptional Analysis of Geobacter

502   Sulfurreducens under Palladium Reducing Conditions Reveals New Key Cytochromes

503   Involved." *Applied Microbiology and Biotechnology* 104(9): 4059–69.

504   Holmes, Dawn E. et al. 2006. "Microarray and Genetic Analysis of Electron Transfer to

505   Electrodes in Geobacter Sulfurreducens." *Environmental Microbiology* 8(10): 1805–15.

506   Inoue, Kengo et al. 2010. "Purification and Characterization of OmcZ , an Outer-Surface ,

507   Octaheme c -Type Cytochrome Essential for Optimal Current Production by Geobacter

508   Sulfurreducens □ †." 76(12): 3999–4007.

509   Jiménez Otero, Fernanda et al. 2021. "Evidence of a Streamlined Extracellular Electron Transfer

510   Pathway from Biofilm Structure, Metabolic Stratification, and Long-Range Electron

511   Transfer Parameters." *Applied and Environmental Microbiology* 87(17).

512   Joshi, Komal, Chi Ho Chan, and Daniel R Bond. 2021. "Geobacter Sulfurreducens Inner

513   Membrane Cytochrome CbcBA Controls Electron Transfer and Growth Yield near the

514   Energetic Limit of Respiration." *Molecular Microbiology* 116(4): 1124–39.

515   https://doi.org/10.1111/mmi.14801.

516   Kim, Byoung-chan Chan et al. 2005. "OmcF , a Putative c -Type Monoheme Outer Membrane

517   Cytochrome Required for the Expression of Other Outer Membrane Cytochromes in

518   Geobacter Sulfurreducens." *Journal of bacteriology* 187(13): 4505–13.

519   Langmead, Ben, and Steven L. Salzberg. 2012. "Fast Gapped-Read Alignment with Bowtie 2."

520   *Nature Methods* 9(4): 357–59.

521   Leang, Ching et al. 2005. "Adaptation to Disruption of the Electron Transfer Pathway for Fe(III)

522   Reduction in Geobacter Sulfurreducens." *Journal of Bacteriology* 187(17): 5918–26.

523   Levar, Caleb E et al. 2017. "Redox Potential as a Master Variable Controlling Pathways of Metal

524   Reduction by Geobacter Sulfurreducens." 11(3): 741–52.

525   http://dx.doi.org/10.1038/ismej.2016.146.

526   Levar, Caleb E, Chi Ho Chan, Misha G Mehta-kolte, and Daniel R Bond. 2014. "An Inner

527   Membrane Cytochrome Required Only for Reduction Of." *mBio* 5(6): 02034–14.

528   Li, Heng et al. 2009. "The Sequence Alignment/Map Format and SAMtools." *Bioinformatics*

529   25(16): 2078–79.

530   Liu, Yimo, James K. Fredrickson, John M. Zachara, and Liang Shi. 2015. "Direct Involvement

531   of OmbB, OmaB, and OmcB Genes in Extracellular Reduction of Fe(III) by Geobacter

532   Sulfurreducens PCA." *Frontiers in Microbiology* 6(OCT): 1–8.

533   Lloyd, Jon R. et al. 2003. "Biochemical and Genetic Characterization of PpcA, a Periplasmic c-

534   Type Cytochrome in Geobacter Sulfurreducens." *Biochemical Journal* 369(1): 153–61.

535   Love, Michael I., Wolfgang Huber, and Simon Anders. 2014. "Moderated Estimation of Fold

536   Change and Dispersion for RNA-Seq Data with DESeq2." *Genome Biology* 15(12): 1–21.

537   Malvankar, Nikhil S. et al. 2011. "Tunable Metallic-like Conductivity in Microbial Nanowire

538   Networks." *Nature Nanotechnology* 6(9): 573–79.

539   Morgado, Leonor et al. 2010. "Thermodynamic Characterization of a Triheme Cytochrome

540   Family From Geobacter Sulfurreducens Reveals Mechanistic And Functional Diversity."

541   *Biophysical Journal* 99(1): 293–301. http://dx.doi.org/10.1016/j.bpj.2010.04.017.

542   Nevin, Kelly P. et al. 2009. "Anode Biofilm Transcriptomics Reveals Outer Surface Components

543   Essential for High Density Current Production in Geobacter Sulfurreducens Fuel Cells."

544   *PLoS ONE* 4(5).

545   Otero, Fernanda Jiménez, and Daniel R. Bond Chi Ho Chan. 2018. "Identification of Different

546   Putative Outer Membrane Electron Conduits Necessary for Fe(III) Citrate, Fe(III) Oxide,

547   Mn(IV) Oxide, or Electrode Reduction by Geobacter Sulfurreducens." *Journal of*

548   *Bacteriology* 200(19): 1–20.

549   Pat-Espadas, Aurora M., Elías Razo-Flores, J. Rene Rangel-Mendez, and Francisco J. Cervantes.

550   2013. "Reduction of Palladium and Production of Nano-Catalyst by Geobacter

551   Sulfurreducens." *Applied Microbiology and Biotechnology* 97(21): 9553–60.

552   Peng, Luo et al. 2016. "Geobacter Sulfurreducens Adapts to Low Electrode Potential for

553   Extracellular Electron Transfer." *Electrochimica Acta* 191: 743–49.

554   http://dx.doi.org/10.1016/j.electacta.2016.01.033.

555   Peng, Luo, and Yong Zhang. 2017. "Cytochrome OmcZ Is Essential for the Current Generation

556   by Geobacter Sulfurreducens under Low Electrode Potential." *Electrochimica Acta* 228:

557   447–52. http://dx.doi.org/10.1016/j.electacta.2017.01.091.

558   Pessanha, Miguel et al. 2006. "Thermodynamic Characterization of Triheme Cytochrome PpcA

559   from Geobacter Sulfurreducens : Evidence for a Role Played in e - / H + Energy

560   Transduction." *Biochemistry* 45: 13910–17.

561   Pokkuluri, P. R. et al. 2011. "Structure of a Novel Dodecaheme Cytochrome c from Geobacter

562   Sulfurreducens Reveals an Extended 12nm Protein with Interacting Hemes." *Journal of*

563   *Structural Biology* 174(1): 223–33. http://dx.doi.org/10.1016/j.jsb.2010.11.022.

564   Richter, Hanno et al. 2009. "Cyclic Voltammetry of Biofilms of Wild Type and Mutant

565   Geobacter Sulfurreducens on Fuel Cell Anodes Indicates Possible Roles of OmcB, OmcZ,

566   Type IV Pili, and Protons in Extracellular Electron Transfer." *Energy and Environmental*

567   *Science* 2(5): 506–16.

568   Salgueiro, Carlos A. et al. 2022. "From Iron to Bacterial Electroconductive Filaments: Exploring

569   Cytochrome Diversity Using Geobacter Bacteria." *Coordination Chemistry Reviews* 452:

570   214284. https://doi.org/10.1016/j.ccr.2021.214284.

571   Santos, Telma C. et al. 2015. "Diving into the Redox Properties of Geobacter Sulfurreducens

572   Cytochromes: A Model for Extracellular Electron Transfer." *Dalton Transactions* 44(20):

573   9335–44. http://www.ncbi.nlm.nih.gov/pubmed/25906375.

574   Shelobolina, Evgenya S. et al. 2007. "Importance of C-Type Cytochromes for U(VI) Reduction

575   by Geobacter Sulfurreducens." *BMC Microbiology* 7(Vi): 1–15.

576   Silva, Marta A., Pilar C. Portela, and Carlos A. Salgueiro. 2021. "Rational Design of

577   Electron/Proton Transfer Mechanisms in the Exoelectrogenic Bacteria Geobacter

578   Sulfurreducens." *Biochemical Journal* 478(14): 2871–87.

579   Torres, César I. et al. 2010. "A Kinetic Perspective on Extracellular Electron Transfer by Anode-

580   Respiring Bacteria." *FEMS Microbiology Reviews* 34(1): 3–17.

581   Torres, César I, Andrew Kato Marcus, Prathap Parameswaram, and Bruce E Rittmann. 2008.

582   "Kinetic Experiments for Evaluating the Nernst-Monod Model for Anode-Respiring

583   Bacteria (ARB) in a Biofilm Anode." *Environmental Science & Technology* 42(17): 6593–

584   97. 10.1021/es800970w.

585   Ueki, Toshiyuki, and Derek R. Lovley. 2009. "Genome-Wide Gene Regulation of Biosynthesis

586   and Energy Generation by a Novel Transcriptional Repressor in Geobacter Species."

587   *Nucleic Acids Research* 38(3): 810–21.

588   Wang, Fengbin et al. 2019. "Structure of Microbial Nanowires Reveals Stacked Hemes That

589   Transport Electrons over Micrometers." *Cell* 177(2): 361-369.e10.

590   https://linkinghub.elsevier.com/retrieve/pii/S0092867419302910.

591   Yalcin, Sibel Ebru et al. 2020. "Electric Field Stimulates Production of Highly Conductive

592   Microbial OmcZ Nanowires." *Nature Chemical Biology* 16(10): 1136–42.

593   http://dx.doi.org/10.1038/s41589-020-0623-9.

594   Yoho, Rachel A., Sudeep C. Popat, and C??sar I. Torres. 2014. "Dynamic Potential-Dependent

595   Electron Transport Pathway Shifts in Anode Biofilms of Geobacter Sulfurreducens."

596   *ChemSusChem* 7(12): 3413–19.

597   Zacharoff, Lori, Chi Ho Chan, and Daniel R. Bond. 2016. "Reduction of Low Potential Electron

598   Acceptors Requires the CbcL Inner Membrane Cytochrome of Geobacter Sulfurreducens."

599   *Bioelectrochemistry* 107: 7–13. http://dx.doi.org/10.1016/j.bioelechem.2015.08.003.

600   Zhu, Xiuping, Matthew D. Yates, and Bruce E. Logan. 2012. "Set Potential Regulation Reveals

601   Additional Oxidation Peaks of Geobacter Sulfurreducens Anodic Biofilms."

602   *Electrochemistry Communications* 22(1): 116–19.

603   http://dx.doi.org/10.1016/j.elecom.2012.06.013.

604